30–300 MeV proton-nucleus total reaction cross sections

B. A. Zelalem,[1,*] F. K. Amanuel,[2] and A. K. Chaubey[1]
[1]*Department of Physics, Addis Ababa University, P.O. Box 1176, Addis Ababa, Ethiopia*
[2]*INFN, Laboratori Nazionali di Legnaro, Legnaro (Padova), Italy*
(Received 24 February 2011; revised manuscript received 29 July 2011; published 12 October 2011)

A functional form has been used to analyze proton total reaction cross sections on stable and unstable target nuclei. For proton or incident nuclei energy per nucleon in the range between 30 and 300 MeV, the parameter values in this functional are interpreted in terms of the nuclear-matter distribution by using reliable total reaction cross-sectional data.

DOI: 10.1103/PhysRevC.84.044606 PACS number(s): 25.40.−h, 24.10.Ht, 21.60.Cs

I. INTRODUCTION

The total reaction cross section (simply called reaction cross section in the following) plays a crucial role in both optical model and statistical model calculations. Since the electron elastic-scattering experiments are yet to be performed on unstable nuclei, and proton elastic-scattering experiments are very limited, the reaction (interaction) cross section remains a fundamental quantity in nuclear reaction experiments, which use radioactive beams [1].

The reaction cross section for sufficiently large projectile energies is directly proportional to the square of the nuclear radius. Therefore, it is an important quantity for studies of nuclear size and matter distributions in nuclei. Understanding of the reaction cross section is also needed in many other research fields; medical physics, radiobiology, cosmic ray, etc. [2].

Recently, there has been much attention given to studies, both theoretical and experimental, of low- and medium-energy nucleon-nucleus scatterings, especially on loosely bound nuclei. Because of limited experimental information on neutron- or proton-rich nuclei, most studies still are performed on stable nuclei; Kox *et al*. [3] gives detailed descriptions. Reaction cross sections for protons have been reproduced by using optical potentials. Koning and Delaroche [4] gave a detailed specification of the phenomenological global optical model, which predicted the latest experimental measurements with various degrees of success [5,6]. Nonetheless, it is utilitarian if one can find a simple functional form so that estimates can be performed quickly, without recourse to computational calculations, which require parameter searches.

Majumdar *et al*. [7] constructed functional forms for proton total cross sections by using predictions of the g-folding microscopic optical potential for nucleon-nucleus scattering in the energy range of 20–300 MeV. The details about the g-folding optical potential and the functional forms are given in Ref. [8] and references therein. The functional forms were also applied to estimate neutron-nucleus total cross sections, with the parameter values themselves expressed as functions of mass and energy [9]. Such work for a proton reaction cross section has not been performed and is considered herein. Also, we link that model to predictions of proton-nucleus reaction cross sections as a function of nuclear-matter radius, by deducing parameters from comparisons of the already tabulated and additional effectual parameter values.

In Sec. II, we review the functional forms of Majumdar *et al*. [7] and Deb and Amos [8,9] and describe the parameter deduction procedures that we follow. Applications and discussion of results are presented in Sec. III. Furthermore, parameters from direct fits to experimental data and those from earlier predictions [8], treated with our deduction scheme, are compared. Finally, we offer conclusions in Sec. IV.

II. FORMULATION

The functional forms for the prediction of the proton-nucleus reaction cross section, expressed as a sum of partial-wave contributions of the scattering (S) matrices, were written [8] as

$$\sigma^{(R)}(E) = \frac{\pi}{k^2}\sum_{l=0}^{\infty}\sigma_l^{(R)}(E). \tag{1}$$

In that paper [8], the partial reaction cross sections, found from the g-folding potential, were compared to and were expressed as

$$\sigma_l^{(R)}(E) = (2l+1)[1+e^{(l-l_o)/a}]^{-1} + \epsilon(2l_o+1)e^{(l-l_o)/a}[1+e^{(l-l_o)/a}]^{-2}. \tag{2}$$

Although one might simply interpolate and/or extrapolate from tabulated values, smoothness of parameters $l_o(E,A)$, $\epsilon(E,A)$, and $a(E,A)$ with energy and mass is convenient for the functional form to be predictive. Such studies have been performed [7–9]. Accordingly, for the proton-nucleus reaction cross section, the parameter ϵ is set as a constant (-1.5) and so, is independent of energy and mass. The variation in $a(E,A)$ is assumed to linearly vary with the center-of-mass momentum (k) as

$$a(E,A) \simeq 1.02k - 0.25, \quad \text{where } k = \frac{1}{\hbar c}\sqrt{E^2 - m^2c^4}. \tag{3}$$

Values of l_o, in Eq. (2), which reproduced experimental data (called direct l_o fits in the following) for a given nucleus across energy, were studied [8]. The direct l_o fits, optimized

*zebelay@gmail.com

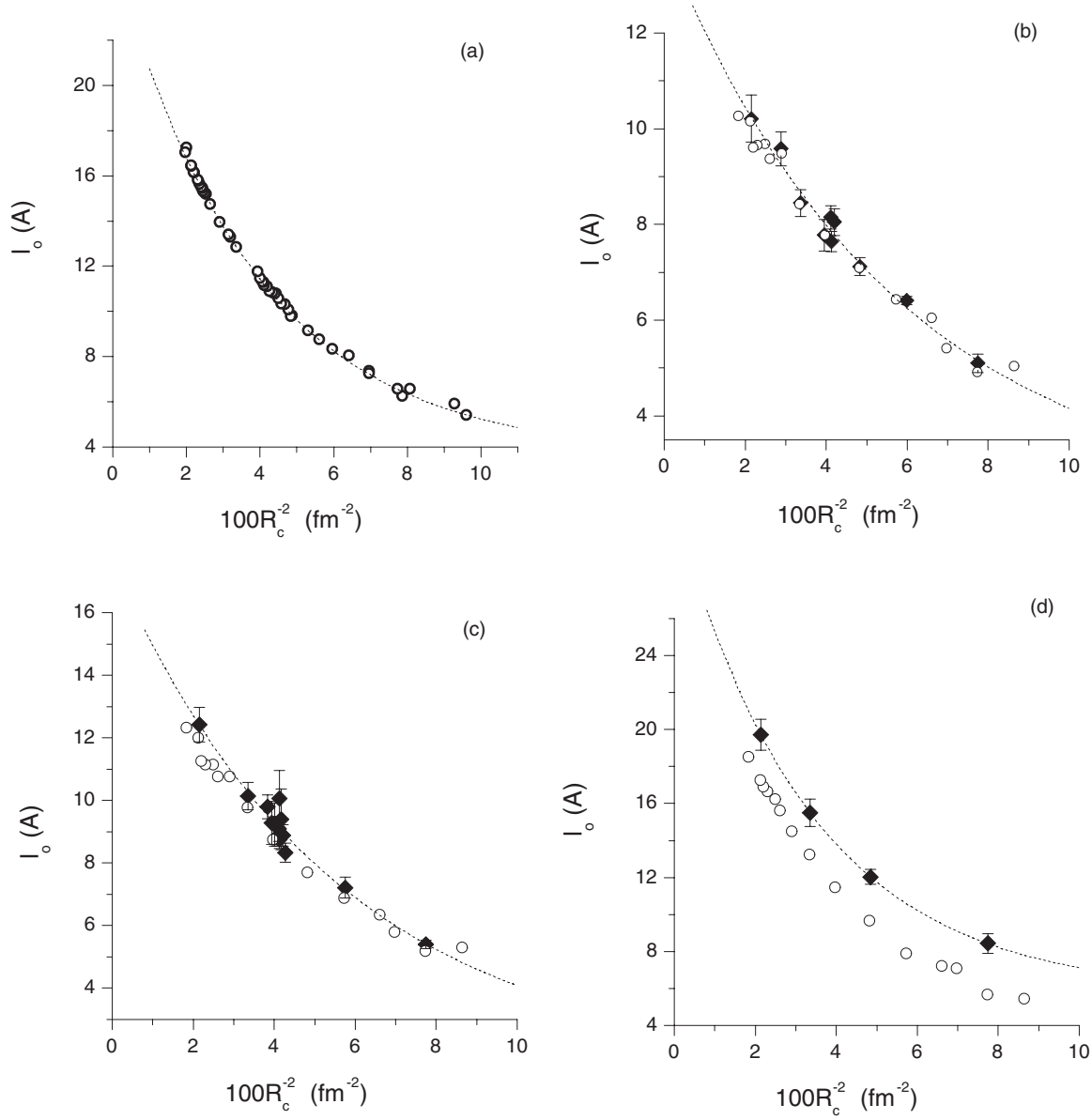

FIG. 1. Variations in direct l_o fits (to the experimental data) are shown by filled diamonds, and the open circles show (a) exact l_o fits to the g-folding potential predictions for 65 MeV protons, and (b)–(d) show optimized l_o fits to experimental data (described in the text), with the inverse square of the nuclear-matter radius (R_c). The dashed curves are found with best-parameter fits to Eq. (6). χ^2 minimization is used.

for optimal smoothness with energy were found to be well behaved, smooth, and somehow linear, except for proton incident energies $E < 50$ MeV [8]. So, good fits to data were possible then with just one parameter specified by interpolating the optimized values [8,9]. However, if further functional properties of l_o can be deduced, then, we may have a most simple to use method by which any required value of the reaction cross section might reasonably be predicted.

In this paper, we investigate that possibility by seeking predictions for isotopes where experimental data are scarce or absent and by deducing parameters from a direct l_o fit and nuclear-matter radii. The nuclear-matter radius that we used, which was related to a black-disk model of scattering, originally was developed [10] to view the nucleus as a black sphere so that a proton-scattering differential cross section would be equivalent to the Fraunhofer diffraction by a circular hole of the same radius embedded in a screen. Then, the nuclear radius could be found from the first proton diffraction peak for the most stable isotopes with masses heavier than 50 [10]. A later paper [1], in constructing a formula for a proton-nucleus reaction cross section, by involving the proton optical depth for the dependence of a cross section on the target mass and proton incident energy, used arguments based on the black-sphere model.

The nuclear-matter radii (R_m), given in Eq. (4), used in this paper are those of a black-sphere model with the

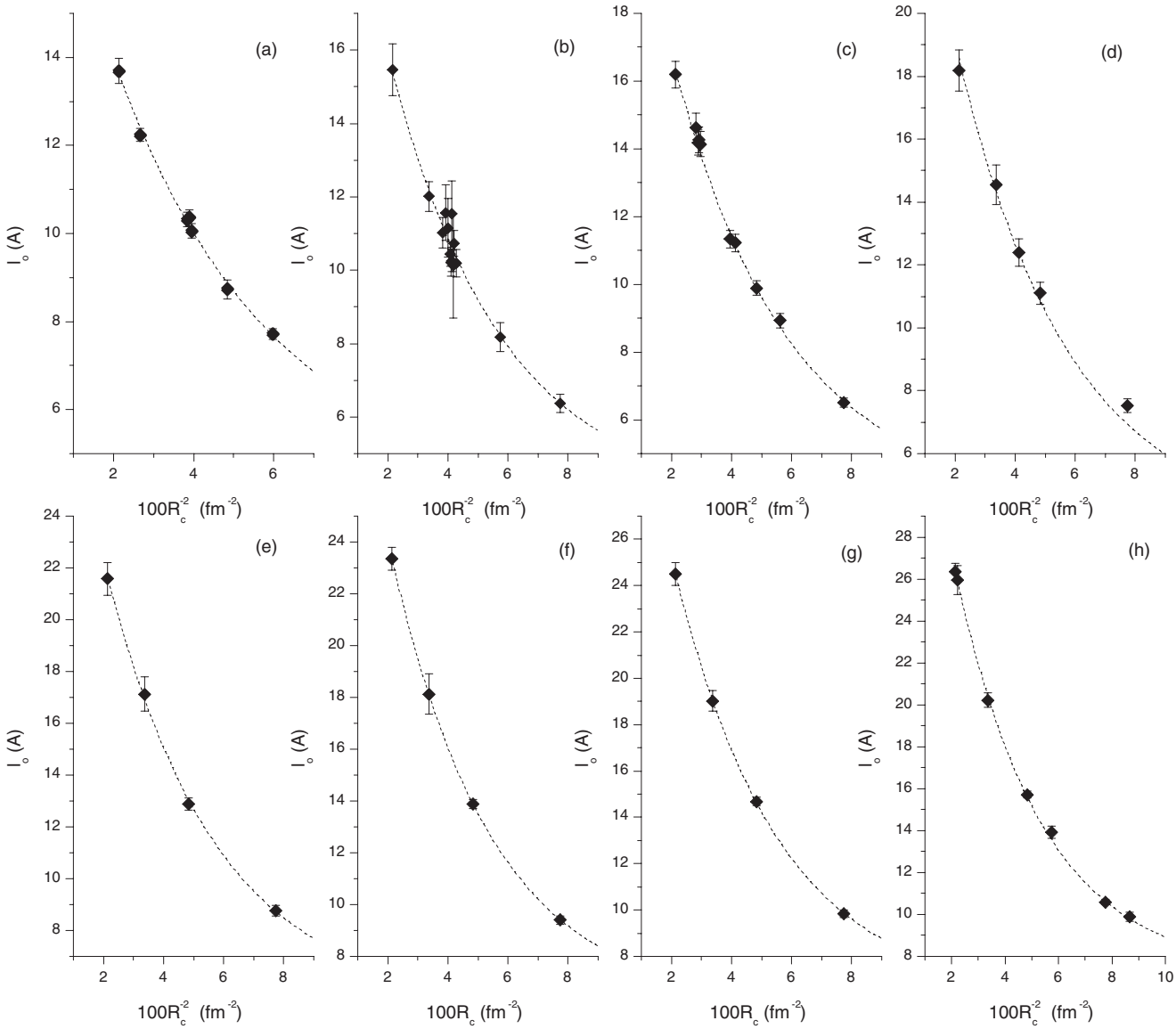

FIG. 2. Variations in direct l_o fits (to experimental reaction cross-sectional data) shown by filled diamonds, with the inverse square of nuclear-matter radius R_c, for proton energies of 48, 60.8, 65.5, 81, 119, 141, 158, and 180 MeV given in Refs. [5,13,14] [shown in panels (a)–(h), respectively]. The dashed curves are obtained from best parameters fit to Eq. (6).

surface-density correction [1] as in Eq. (5),

$$R_m = \sqrt{\frac{N}{A}R_n^2 + \frac{Z}{A}R_p^2}, \tag{4}$$

where the matter radii for the proton and neutron, R_p and R_n, are given as

$$R_p = c_1 A^{1/3} + c_2 + c_3(\delta - \delta_o)^2,$$
$$R_n = c_4 A^{1/3}(1 + c_5 L\delta^2 + c_6 L^2\delta^4) + c_7 + c_8\delta.$$

In Eq. (5), D is a thickness parameter, which is taken to be 2.2 fm, $\delta = 1 - 2Z/A$ is the neutron excess, and $L = 100$ MeV is a typical value of the density symmetry coefficient. The other parameter values are $\delta_o = 0.880$, $c_1 = 0.915$ fm, $c_2 = -0.102$ fm, $c_0 = 0.389$ fm, $c_4 = 0.880$ fm, $c_5 = 0.006\,35$ MeV^{-1}, $c_6 = -0.000\,172$ MeV^{-2}, $c_7 = 0.302$ fm, and $c_8 = 0.193$ fm,

$$R \simeq R_m + \frac{D}{2} - R_m\left(1 + \frac{12R_m^2}{D^2}\right)^{-1}. \tag{5}$$

The nuclear-matter radius, found from Eq. (5), is corrected by a scale factor of $R_m(A,\delta)/R_m\,(A,\delta = 0)$, where the denominator is the nuclear-matter radius calculated for the $Z = N = A/2$ system. A similar correction has been used to take the effect of the asymmetry coefficient at finite neutron excess [1] into account. We denote the nuclear radius, which results after this correction, as R_c.

Our empirical observation, of the dependence of the inverse square of R_c on the exact l_o values, which are fit to proton reaction cross sections calculated from g-folding potentials

TABLE I. Best-parameter-fit values at each incident proton laboratory energy. The χ^2 of the fit is given in the last column.

Energy (MeV)	l_o^o (dimensionless)	c_o	t (fm^{-2})	χ^2
30.0	2.114	11.841	5.704	0.077
40.0	1.455	16.197	5.500	0.063
48.0	4.179	16.407	3.871	0.025
60.8	3.785	20.802	3.711	0.184
65.5	3.614	22.254	3.821	0.053
81.0	3.627	26.571	3.711	0.024
100.0	5.767	26.275	3.379	0.000
119.0	5.189	29.646	3.641	0.053
141.0	6.119	32.509	3.378	0.000
158.0	6.229	33.914	3.464	0.008
180.0	7.210	36.955	3.257	0.052

for 65 MeV [11], is indicated in panel (a) of Fig. 1. Here, the target nuclei range from ^{6}Li to ^{238}U. Of note is that, at this energy, cross sections of light neutron-rich nuclei ^{7,9,11}Li and ^{11}B are predicted with less than 10% error. The dashed curve in Fig. 1 is found through best-parameter fits (l_o^o, c_o, and t) to Eq. (6). A χ^2 minimization was used,

$$l_o = l_o^o + c_o e^{-R_c^{-2}/t}. \quad (6)$$

The parameter fits fixed in this way reproduced l_o [by using Eq. (6)] to its exact fit values with errors less than 2.4%. Exceptions are lithium isotopes ^{7,9,11}Li, ^{11}B, and ^{53}Fe, for which errors range from 2.5% to 5.2%. For the cases studied, parameter l_o has a simple exponential form, as in Eq. (6), for proton energy $E > 30$ MeV.

The functional form for the partial cross section, Eq. (2), is simply a conventional form, which is adopted for the corresponding quantity that is found from the moduli of the S matrices for a proton that interacts with the g-folding potential. However, from the perspective of the microscopic model, the reaction cross section is described by radii of interacting nuclei and the transmission of the target toward the projectile [3]. Transmission of the interior (core) of the nuclei effectively is unity, regardless of the form of density distribution, which is chosen for the core-overlap region. Therefore, for the other two parameters [$\epsilon(E, A)$ and $a(E, A)$], which are specified as described above, strong dependence of l_o on the nuclear radius and nuclear-matter distribution beyond the core region (textures of nuclear surface) is expected for a given incident energy (per nucleon).

III. APPLICATION AND DISCUSSION

Specifics of the functional forms were deduced by using properties of the nuclei, ^{9}Be, ^{12}C, ^{16}O, ^{19}F, ^{27}Al, ^{40}Ca, ^{63}Cu, ^{90}Zr, ^{118}Sn, ^{140}Ce, ^{159}Tb, ^{181}Ta, ^{197}Au, ^{208}Pb, and ^{238}U. Parameter values were fixed by optimizing fits to experimentally measured cross-sectional data across the energy for each nucleus [8]. The tabulated l_o values (referred as optimized fits in the following) for each of the above nuclei at 30, 40, 50, 60, 70, 80, 90, 100, 150, 250, and 300 MeV

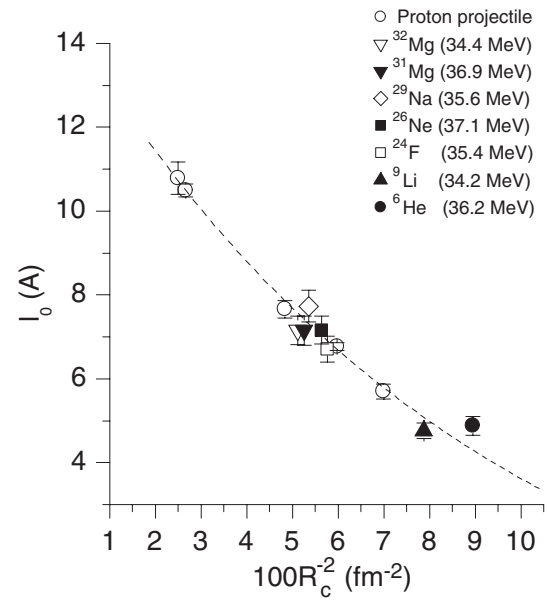

FIG. 3. Direct l_o fits for projectiles and energy (per nucleon) shown in the legends for data in Ref. [15]. The l_o values fixed from Eq. (6) with best-parameter fits for the 35 MeV proton (incident on stable targets) are shown by the dashed curve. Direct l_o fits for these reaction cross-sectional data [13] are also shown by open circles.

proton energies [12], along with direct l_o fits for many nuclei, which include those listed above, have been interpreted in the form, which is given in Eq. (6). Panels (b)–(d) of Fig. 1 show the direct l_o fits by filled diamonds and show the optimized fits by open circles.

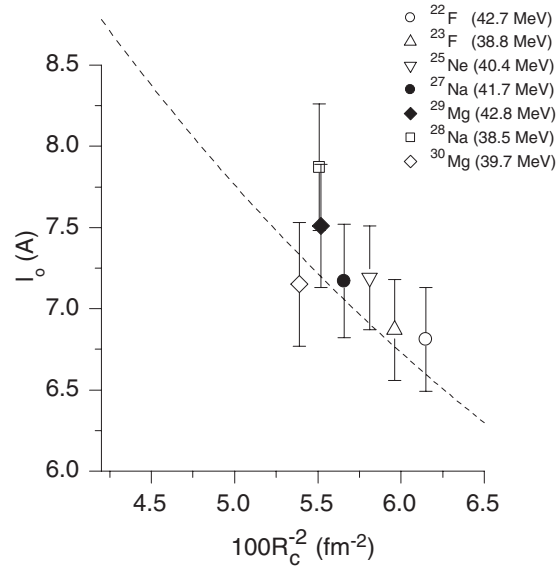

FIG. 4. Direct l_o fit for incident nuclei and energy per nucleon shown in the legends given in Ref. [15]. The dashed curve is the best fit for the 40 MeV protons reaction cross section of stable nuclei (numerical values are given in Table I).

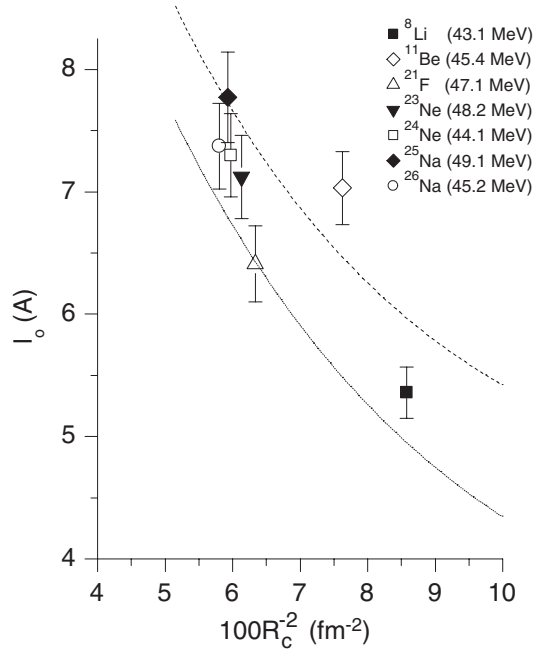

FIG. 5. Direct l_o fits for incident nuclei and energy per nucleon shown in the legends [15]. The lower curve, shown by the dotted line, and the upper dashed curve are found from Eq. (6) for 40 and 48 MeV respective parameter fits (numerical values are given in Table I).

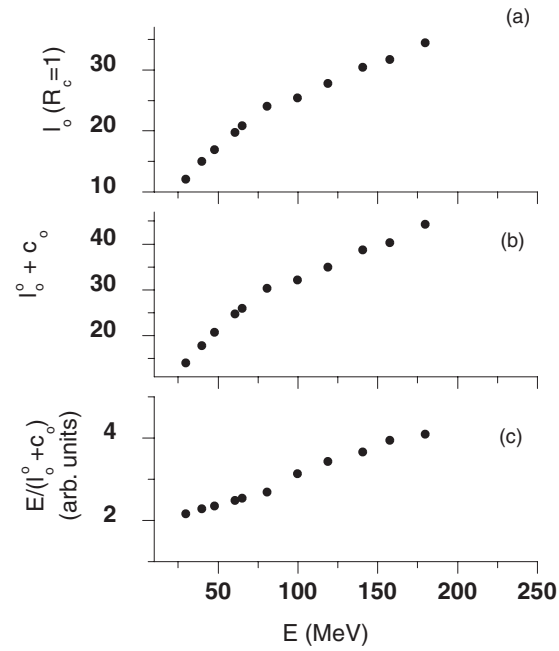

FIG. 6. Variations of best-fit parameters in Eq. (6), given in Table I, with energy.

Fits to the lower and upper limits of the reported experimental uncertainties are used to find the errors on direct l_o fits. In panel (b) of Fig. 1, the variations in direct l_o fits with R_c to 30 MeV proton data incident on ^{12}C, ^{24}Mg, ^{40}Ca, ^{56}Fe, ^{58}Ni, ^{59}Co, ^{60}Ni, ^{90}Zr, ^{120}Sn, and ^{208}Pb are shown. Calculations made by using Eq. (6) match those direct l_o fits within the experimental error bars. That is also the case with the direct l_o fits for 40 MeV proton data as shown in panel (c). Here, the direct l_o fits are performed for ^{12}C, ^{27}Al, ^{56}Fe, ^{57}Fe, ^{58}Fe, ^{58}Ni, ^{59}Co, ^{60}Ni, ^{62}Ni, ^{64}Ni, ^{68}Zn, ^{90}Zr, and ^{208}Pb. These data are taken from Ref. [13].

The situation is different at 100 MeV, where direct l_o fits to the recently reported ^{12}C, ^{40}Ca, ^{90}Zr, and ^{208}Pb proton reaction cross-sectional data [5] are compared with optimized fits. Optimized fits, at this energy, showed systematic deviations from direct l_o fits, while the parameters followed the proposed form, Eq. (6). This discrepancy is shown in Ref. [8] as a deviation of predictions (of the functional forms) from that of the g-folding potential and/or to the experimental data.

The scheme, which is proposed here, Eq. (6), is tested by using all the 48, 60.8, 65.5, 81, 119, 141, 158, and 180 MeV energy proton reaction cross-sectional data, Refs. [5,13,14], and the results are displayed in Fig. 2. Numerical values of parameter fits [values of l_o^o, c_o, and t in Eq. (6)], at each energy considered here, are also tabulated in Table I.

Furthermore, direct l_o fits to the data in Ref. [15] are separately compared, in Figs. 3–5 to Eq. (6), with parameter fits for the incident energy per nucleon closer to the proton energy considered. Direct l_o fits for data in Ref. [15] are performed as if these cross sections are for protons of energy equal to the energy per nucleon of the projectile, which, in this case, are considered as targets in reverse. Otherwise, the same parameter specifications, discussed above, are applied. In Fig. 3, direct l_o fits for the measurements of de Vismes *et al.* [15] on neutron-rich unstable nuclei: ^{9}Li, ^{32}Mg, ^{24}F, ^{29}Na, ^{6}He, ^{31}Mg, and ^{26}Ne at around 35 MeV per nucleon incident energy and for the data of 35 MeV proton reaction cross sections, which are incident on stable nuclei [13], are compared.

Similar comparisons of direct l_o fits, for the data of de Vismes *et al.* [15] for incident energy per nucleon, which ranges from 38.5 to 42.8 MeV with direct l_o fits for 40 MeV data on stable nuclei and for incident energy per nucleon, which ranges from 43.1 to 49.1 MeV, with direct l_o fits for 40 and 48 MeV data on stable nuclei, are presented in Figs. 4 and 5, respectively. Direct l_o fits of data from stable target nuclei and radioactive incident nuclei are in complete resemblance at equal energy (per nucleon) when treated by this scheme, Eq. (6). The same is true for the proton reaction cross section for ^{4}He, incident at 81.1 MeV per nucleon on the proton target, when treated with the reaction cross section of stable nuclei for the proton energy of 81 MeV (not shown here). Inclusion of data, in the search for random parameter fits, alters the parameter values tabulated in Table I. This is especially so in the case where one includes data from incident light nuclei, such as ^{4}He, which does not fall in the general systematic because of its special nature [15]. This is why the best-fit parameters in Table I are performed by using data in which protons are incident on stable nuclei only, therefore, consistency across energy can be maintained.

Special nuclear surface structures, such as halo nuclear-matter distributions, are not taken into account by the present scheme, Eq. (6). This could be one of the reasons for the deviations of fits for the data of ^{28}Na (38.5 MeV), shown in

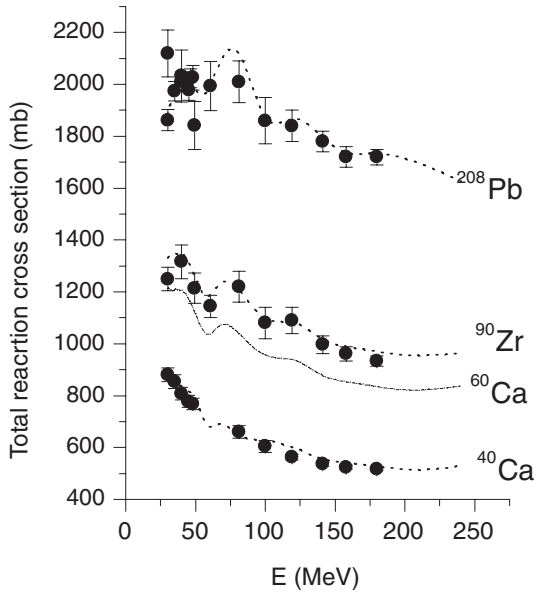

FIG. 7. Predictions, which use interpolated values of the parameters in Eq. (6), are shown by dotted curves, and experimental data [5,13] are shown by filled circles for corresponding nuclei at the right end of each curve. The dot-dashed curve is the prediction for ^{60}Ca, for which no experimental data are shown.

Fig. 4, ^{11}Be (45.4 MeV) and ^{21}F (47.1 MeV), shown in Fig. 5, from the general trends. The unusual natures of ^{11}Be and ^{28}Na had been observed in previous studies and were attributed to the presence of a halo or neutron skin in these nuclei [15].

With no particular physical constraint sought, parameters in Eq. (6), fixed through the direct l_o fits to sparse data, in energy and mass, remain random and highly dependent on the data considered. Therefore, a general energy dependence of parameters, the mass variation, which has been fixed by Eq. (6), requires more complete studies, which involve many targets and/or projectiles and energy. However, from Eq. (6), one gets the analytic form for R_c, which is dependent only on the projectile-target system, and with smooth variations in $c_o + l_o^o$ and $E/(c_o + l_o^o)$, as shown in Fig. 6, simple extrapolations or interpolations are possible. We also show a variation in l_o for $R_c = 1$ in panel (a) of Fig. 6. These were used to give better predictions, from an earlier application of the functional form [5], on the latest ^{90}Zr and ^{208}Pb data, while maintaining the good predictions for the reaction cross section of ^{40}Ca, shown in Fig. 7. Our predictions, shown by dotted curves in Fig. 7, were collected through a spline interpolation of parameter c_o and variations shown in Fig. 6 to find the remaining two parameters in Eq. (6). Predictions of this model for ^{60}Ca, an isotope in the vicinity of the neutron drip line, are also shown in Fig. 7.

IV. CONCLUSION

On the basis of the limited and sparse sets of nuclei and energy considered, parameters in the functional forms for the total reaction cross section for the proton projectile energy between 30 and 300 MeV, or for an equivalent (in energy per nucleon) incident nucleus on a proton, have been interpreted in terms of nuclear-matter distribution, corrected for surface thickness and symmetry, from the black-disk model. The reaction cross-sectional data, from both stable and neutron-rich unstable nuclei are treated identically and are predicted within error bars. The unusual natures of ^{11}Be and ^{28}Na, observed in previous studies, are also observed, in this paper, as a deviation from the simple trends that the parameter, in the functional, follow with nuclear-matter distributions, in support of the presence in these nuclei of a halo or neutron skins [15].

The scheme followed for the data of de Vismes *et al.* [15] and Eq. (6) allowed similar treatments of the proton reaction cross-sectional data from stable (target) and neutron-rich unstable (projectile) nuclei. This is expected, for, in this energy range, the nuclear reactions are addressed in terms of individual nucleon-nucleon collisions [3].

Extrapolation or interpolation to regions where data are scarce can easily be performed from tabulated parameters. Use of the smooth energy variations, shown in Fig. 6, as a control, for consistency, and for the interpolation of the parameters, demonstrated better predictions for the target nuclei considered here, shown in Fig. 7, by taking local energy variations into account.

This model provides vast alternatives for obtaining a prediction, where experimental data are scarce or absent and for a study on new reaction cross-sectional measurements for the smooth behavior with existing data at a given energy and/or across mass, which may easily be examined. An additional advantage of this scheme is that it can also be used to supplement starting information on partial cross sections as required on occasions of optical model developments and in the analysis of the experimental measurements of reaction cross sections as defined in Ref. [5].

ACKNOWLEDGMENTS

We are grateful to Professor A. K. Amos for many useful discussions as well as for critical comments made during the preparation of this paper.

[1] K. Iida, A. Kohama, and K. Oyamatsu, J. Phys. Soc. Jpn. **76**, 044201 (2007).
[2] C.-T. Liang, Y.-A. Luo, X.-H. Li, and C.-H. Cai, J. Phys. G **47**, 015102 (2009).
[3] S. Kox *et al.*, Phys. Rev. C **35**, 1678 (1987).
[4] A. J. Koning and J. P. Delaroche, Nucl. Phys. A **713**, 231 (2003).
[5] A. Auce *et al.*, Phys. Rev. C **71**, 064606 (2005).
[6] P. Mermod *et al.*, Phys. Rev. C **74**, 054002 (2006).

[7] S. Majumdar, P. K. Deb, and K. Amos, Phys. Rev. C **64**, 027603 (2001).
[8] P. K. Deb and K. Amos, Phys. Rev. C **67**, 067602 (2003).
[9] P. K. Deb and K. Amos, Phys. Rev. C **69**, 064608 (2004).
[10] A. Kohama, K. Iida, and K. Oyamatsu, Phys. Rev. C **69**, 064316 (2004).
[11] P. J. Dortmans, K. Amos, S. Karataglidis, and J. Raynal, Phys. Rev. C **58**, 2249 (1998).
[12] K. Amos (private communication).
[13] W. Bauhoff, At. Data Nucl. Data Tables **35**, 429 (1986).
[14] A. Ingemarsson *et al*., Nucl. Phys. A **653**, 341 (1999).
[15] A. de Vismes *et al*., Nucl. Phys. A **706**, 295 (2002).